Full Eulerian lattice Boltzmann model for conjugate heat transfer

Yang Hu* and Decai Li†
School of Mechanical, Electronic and Control Engineering, Beijing Jiaotong University, Beijing 100044, People's Republic of China

Shi Shu
School of Mathematics and Computational Science, Xiangtan University, Xiangtan 411105, People's Republic of China

Xiaodong Niu
College of Engineering, Shantou University, Shantou 515063, People's Republic of China

(Received 8 August 2015; revised manuscript received 1 November 2015; published 10 December 2015)

In this paper a full Eulerian lattice Boltzmann model is proposed for conjugate heat transfer. A unified governing equation with a source term for the temperature field is derived. By introducing the source term, we prove that the continuity of temperature and its normal flux at the interface is satisfied automatically. The curved interface is assumed to be zigzag lines. All physical quantities are recorded and updated on a Cartesian grid. As a result, any complicated treatment near the interface is avoided, which makes the proposed model suitable to simulate the conjugate heat transfer with complex interfaces efficiently. The present conjugate interface treatment is validated by several steady and unsteady numerical tests, including pure heat conduction, forced convection, and natural convection problems. Both flat and curved interfaces are also involved. The obtained results show good agreement with the analytical and/or finite volume results.

DOI: 10.1103/PhysRevE.92.063305 PACS number(s): 47.11.−j, 44.35.+c, 47.55.N−, 44.05.+e

I. INTRODUCTION

Heat transfer between different mediums is frequently encountered in many engineering application fields, such as cooling of microelectronic devices, heat exchangers, and chemical and nuclear reactors. In the past few decades, conjugate heat transfer has been investigated by many researchers theoretically and experimentally. In addition to the theoretical and experimental methods, the computer simulation technique is an effective and reliable research approach. Through solving the governing equation of the temperature field and implementing the conjugate interface conditions, the details of the temperature distribution can be obtained. In fact, the numerical works of the conjugate heat transfer based on convectional computational fluid dynamics methods have been done by many scholars.

The lattice Boltzmann method (LBM) has been a popular kinetic scheme in recent years. Via simple algebraic manipulations, many complex fluid systems can be simulated. Now LBM has been proved to be a competitive and composing numerical simulation tool for incompressible flows, and it has been applied successfully in multicomponent-multiphase flows [1,2], turbulence flows [3,4], microflows [5,6], fluid-solid interactions [7–11], porous media flows [12–14], and thermal flows [15–18]. The efforts of simulation of conjugate heat transfer using LBM have been also considered in some open literature. The first attempt to study this issue was done by Wang *et al.* [19]. They proposed a "half lattice division" treatment for fluid-solid conjugate interface conditions. Although there are not any additional treatments near the fluid-solid interface, however, this method is limited to the steady cases [19,20]. Meng *et al.* presented a counter-slip scheme which assumes that the unknown energy distributions of the fluid and solid are in equilibrium with the counter-slip internal energy [21]. Meng *et al.* used this method to simulate the conjugate heat transfer in high-frequency oscillating flows. Seddiq *et al.* also developed a scheme to solve the conjugate heat transfer problems by the LBM [22]. In this method, they assumed that the ratio of the gradient of the distribution functions is proportional to the reverse of the thermal conductivities ratio. However, as pointed out in Ref. [23], the above assumption of proportionality on the distribution function has not been proved. In fact, all the above interface schemes based on the LB model for conjugate heat transfer can only be applied in straight-interface geometry. To overcome this drawback, Hu *et al.* extend the LBM in combination with the immersed boundary method to simulate the fluid-solid conjugate heat transfer problems in complex geometries. However, only steady cases can be simulated [24]. Li *et al.* proposed an approach based on their generalized framework for thermal boundary condition treatments [23,25]. This treatment preserves second-order accuracy for arbitrary link fractions. Li *et al.* applied their method to simulate some numerical examples successfully, including steady and unsteady flows with conjugate heat transfer. Le *et al.* also developed a conjugate interface method by performing extrapolations along the normal direction [26]. They argued that the normal heat flux across the interface cannot be computed directly. This indicates that some important parameters cannot be calculated. The basic idea of their method is to determine the transport scalar value at the interface by extrapolations from the two separate domains toward the interface along the normal direction. Then the conjugate boundary condition can be transferred to a Dirichlet boundary condition. Then the corresponding approach for a Dirichlet boundary condition can be used.

In this paper, a full Eulerian lattice Boltzmann model for conjugate heat transfer is proposed. A unified governing

*hy304@126.com
†Corresponding author: dcli@bjtu.edu.cn

equation with a source term is built to model the temperature field in both fluid and solid regions. We prove that the continuity conditions of the temperature and normal heat flux are satisfied automatically. In our scheme, the curved interface is treated as the zigzag lines. It need not track to the Lagrangian points or points of intersection between the grid lines and the curved interface. As a result, the present solution procedure does not require complicated treatment near the interface and is independent of the interface topology. The present method has a great potential to simulate a heat transfer system with complex and time-dependent interfaces. It should be noted that Karani and Huber also proposed a full Eulerian LB model for conjugate heat transfer in heterogeneous media [27]. However, according to our study, there exist two theoretical drawbacks in their method. One is that this method lacks mathematical rigor in deriving the evolution equation of the temperature field. Another drawback is that the numerical results of this method show the dependence of the discrete scheme on the heat capacitance.

The present LB model is examined by some test cases. Both steady-state and transient conjugate heat transfer problems are considered. It is found that the present results agree well with the analytical or finite volume solutions. The remainder of this paper is organized as follows. Section II presents the mathematical foundation of the present LB model. The details of the present conjugate interface treatment are discussed in Sec. III. Section IV provides the numerical results and discussion.

II. MATHEMATICAL FORMULA

As shown in Fig. 1, the fluid-solid conjugate heat transfer problem is considered. The entire computational domain is composed by the fluid region Ω_1 and solid region Ω_2. The fluid-solid interface is denoted by Γ. $\mathbf{n}$ is the unit outward normal vector on Γ. The fluid and solid materials have different thermophysical properties, such as density, ρ, thermal conductivity, κ, and specific heat capacity, c_p. The governing equation of temperature field on $\Omega_1 \cup \Omega_2$ can be written as

$$\frac{\partial T}{\partial t} + \nabla \cdot (\mathbf{u}T) = \nabla \cdot (\chi \nabla T), \tag{1}$$

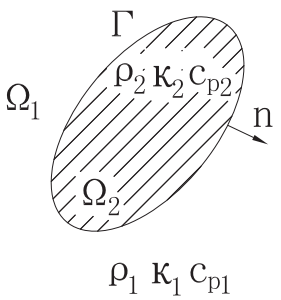

FIG. 1. A diagram of geometry for conjugate heat transfer problems.

where T and $\mathbf{u}$ are the temperature and velocity, respectively. χ is the thermal diffusivity and is defined as

$$\chi(\mathbf{x}) = \begin{cases} \frac{\kappa_1}{(\rho c_p)_1}, & \mathbf{x} \in \Omega_1, \\ \frac{\kappa_2}{(\rho c_p)_2}, & \mathbf{x} \in \Omega_2. \end{cases} \tag{2}$$

The conjugate interface conditions are given by

$$T_1|_\Gamma = T_2|_\Gamma, \tag{3}$$

$$\kappa_1 \frac{\partial T_1}{\partial n}\bigg|_\Gamma = \kappa_2 \frac{\partial T_2}{\partial n}\bigg|_\Gamma. \tag{4}$$

In this study, a source term or correction term q is introduced to implement the above conjugate interface conditions. The modified governing equation can be written as

$$\frac{\partial T}{\partial t} + \nabla \cdot (\mathbf{u}T) = \nabla \cdot (\chi \nabla T) + q, \tag{5}$$

$$q = \int_\Gamma \delta Q \delta(\mathbf{x} - \mathbf{X}) ds, \tag{6}$$

where δ is the Dirac function. δQ is the heat flux across the interface Γ. s is the arc-length parameter. Actually, inclusion of a source term in the governing equation to implement the boundary condition is widely used in the immersed boundary method (IBM), immersed interface method, and distributed Lagrange multiplier–fictitious domain method.

In fact, we can prove that the heat flux δQ can be expressed as

$$\delta Q = -\kappa_1 \frac{\partial T_1}{\partial n}\bigg|_\Gamma \left[\frac{1}{\rho c_p}\right] = -\kappa_2 \frac{\partial T_2}{\partial n}\bigg|_\Gamma \left[\frac{1}{\rho c_p}\right], \tag{7}$$

where the square brackets [ ] are the jump function across the interface Γ, and it is denoted by

$$[\Phi(\mathbf{X})] = \lim_{\epsilon \to 0^+} [\Phi(\mathbf{X} + \epsilon \mathbf{n}) - \Phi(\mathbf{X} - \epsilon \mathbf{n})]. \tag{8}$$

In the following section, the above interface relation [Eq. (7)] is derived. Based on the previous study [17], we have the following jump conditions:

$$[T] = 0, \tag{9}$$

$$\delta Q = -\left[\chi \frac{\partial T}{\partial n}\right]. \tag{10}$$

Obviously, Eq. (9) indicates that the temperature is continuous across the interface Γ.

From Eqs. (7) and (10), we can get

$$\frac{\kappa_1}{(\rho c_p)_1} \frac{\partial T_1}{\partial n}\bigg|_\Gamma - \frac{\kappa_2}{(\rho c_p)_2} \frac{\partial T_2}{\partial n}\bigg|_\Gamma = \frac{\kappa_2}{(\rho c_p)_1} \frac{\partial T_2}{\partial n}\bigg|_\Gamma - \frac{\kappa_2}{(\rho c_p)_2} \frac{\partial T_2}{\partial n}\bigg|_\Gamma. \tag{11}$$

Further, Eq. (11) can be simplified as

$$\kappa_1 \frac{\partial T_1}{\partial n}\bigg|_\Gamma = \kappa_2 \frac{\partial T_2}{\partial n}\bigg|_\Gamma. \tag{12}$$

As expected, we found that the continuity of normal heat flux can be ensured. The proof is completed.

Moreover, without considering the heat source term, that is,

$$\delta Q = -\left[\chi \frac{\partial T}{\partial n}\right] = 0. \tag{13}$$

It denotes

$$\chi_1 \frac{\partial T}{\partial n}\bigg|_\Gamma = \chi_2 \frac{\partial T}{\partial n}\bigg|_\Gamma. \tag{14}$$

If the ratio of thermal conductivities is not equal to the ratio of thermal diffusivities, we cannot obtain the correct solution. The present conclusion is consistent with the analysis in Ref. [27].

III. NEW LATTICE BOLTZMANN MODEL FOR CONJUGATE HEAT TRANSFER

The D2Q9 lattice model is selected as an example to describe the present algorithm, and the corresponding discrete velocity set is defined as

$$\mathbf{e}_\alpha = \begin{cases} (0,0), & \alpha = 0 \\ \left(\cos\left[(\alpha-1)\frac{\pi}{2}\right], \sin\left[(\alpha-1)\frac{\pi}{2}\right]\right)c, & \alpha = 1,2,3,4 \\ \sqrt{2}\left(\cos\left[(2\alpha-1)\frac{\pi}{4}\right], \sin\left[(2\alpha-1)\frac{\pi}{4}\right]\right)c, & \alpha = 5,6,7,8, \end{cases} \tag{15}$$

where $c = \Delta x/\Delta t$; Δx is the lattice spacing and Δt is the time step. In the case of $\Delta x = \Delta t$, c is set as 1.

In recent years, many LB models for convection-diffusion equations (CDEs) have been proposed [28–31]. The following multirelaxation-time LB model is chosen as the temperature field solver [30]. The evolution equation with source term can be written as

$$\mathbf{g}(\mathbf{x}+\mathbf{e}_\alpha\Delta t, t+\Delta t) - \mathbf{g}(\mathbf{x},t) = -\mathbf{M}^{-1}\mathbf{S}_g[\mathbf{m}(\mathbf{x},t) - \mathbf{m}^{\mathrm{eq}}(\mathbf{x},t)] + \Delta t\mathbf{M}^{-1}\left(\mathbf{I} - \frac{\mathbf{S}_g}{2}\right)\mathbf{Q}(\mathbf{x},t), \tag{16}$$

where the above notations denote

$$\mathbf{g}(\mathbf{x},t) = (g_0(\mathbf{x},t), g_1(\mathbf{x},t), \ldots, g_8(\mathbf{x},t))^T, \tag{17}$$

$$\mathbf{m}(\mathbf{x},t) = \mathbf{M}\mathbf{g} = (m_0(\mathbf{x},t), m_1(\mathbf{x},t), \ldots, m_8(\mathbf{x},t))^T, \tag{18}$$

$$\mathbf{m}^{\mathrm{eq}}(\mathbf{x},t) = \left(m_0^{\mathrm{eq}}(\mathbf{x},t), m_1^{\mathrm{eq}}(\mathbf{x},t), \ldots, m_8^{\mathrm{eq}}(\mathbf{x},t)\right)^T, \tag{19}$$

$$\mathbf{Q}(\mathbf{x},t) = (Q_0(\mathbf{x},t), Q_1(\mathbf{x},t), \ldots, Q_8(\mathbf{x},t))^T. \tag{20}$$

Here $g_\alpha(\mathbf{x},t)$ is the temperature distribution function for the discrete velocity $\mathbf{e}_\alpha$. $\mathbf{M}$ is the orthogonal transformation matrix and it can be constructed by

$$\mathbf{M} = \begin{pmatrix} 1 & 1 & 1 & 1 & 1 & 1 & 1 & 1 & 1 \\ -4 & -1 & -1 & -1 & -1 & 2 & 2 & 2 & 2 \\ 4 & -2 & -2 & -2 & -2 & 1 & 1 & 1 & 1 \\ 0 & 1 & 0 & -1 & 0 & 1 & -1 & -1 & 1 \\ 0 & -2 & 0 & 2 & 0 & 1 & -1 & -1 & 1 \\ 0 & 0 & 1 & 0 & -1 & 1 & 1 & -1 & -1 \\ 0 & 0 & -2 & 0 & 2 & 1 & 1 & -1 & -1 \\ 0 & 1 & -1 & 1 & -1 & 0 & 0 & 0 & 0 \\ 0 & 0 & 0 & 0 & 0 & 1 & -1 & 1 & -1 \end{pmatrix}. \tag{21}$$

$\mathbf{S}_g$ is the relaxation matrix in the moment space and it is given by

$$\mathbf{S}_g = \begin{pmatrix} \sigma_0 & 0 & 0 & 0 & 0 & 0 & 0 & 0 & 0 \\ 0 & \sigma_1 & 0 & 0 & 0 & 0 & 0 & 0 & 0 \\ 0 & 0 & \sigma_2 & 0 & 0 & 0 & 0 & 0 & 0 \\ 0 & 0 & 0 & \sigma_3 & (\sigma_3/2-1)\sigma_4 & 0 & 0 & 0 & 0 \\ 0 & 0 & 0 & 0 & \sigma_4 & 0 & 0 & 0 & 0 \\ 0 & 0 & 0 & 0 & 0 & \sigma_5 & (\sigma_5/2-1)\sigma_6 & 0 & 0 \\ 0 & 0 & 0 & 0 & 0 & 0 & \sigma_6 & 0 & 0 \\ 0 & 0 & 0 & 0 & 0 & 0 & 0 & \sigma_7 & 0 \\ 0 & 0 & 0 & 0 & 0 & 0 & 0 & 0 & \sigma_8 \end{pmatrix}. \tag{22}$$

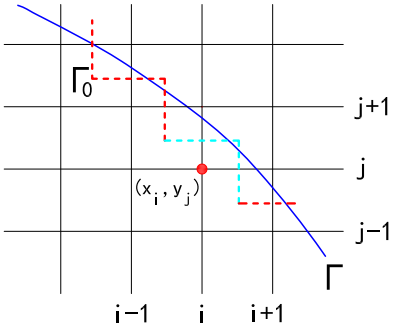

FIG. 2. (Color online) A diagram of geometry for a curved interface and a staircase interface.

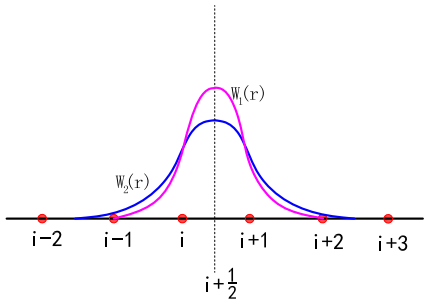

FIG. 3. (Color online) Schematic of two different discrete delta functions.

It should be noticed that $\mathbf{S}_g$ is not a diagonal matrix. As asserted in Ref. [30], the additional deviation term in the recovered macroscopic equation can be eliminated. Here, the elements in matrix $\mathbf{S}_g$ are determined by

$$\sigma_0 = 0, \quad \sigma_1 = \sigma_2 = \sigma_4 = \sigma_6 = \sigma_7 = \sigma_8 = 1, \qquad \sigma_3 = \sigma_5 = \frac{\Delta t}{3\chi/c + 0.5\Delta t}. \tag{23}$$

The equilibrium moment $\mathbf{m}^{\mathrm{eq}}$ is

$$\mathbf{m}^{\mathrm{eq}} = (T, -2T, 2T, uT, -uT, vT, -vT, 0, 0). \tag{24}$$

The discrete heat source or sink term $\mathbf{Q}$ in Eq. (16) is obtained by

$$\mathbf{Q} = (q, -2q, 2q, 0, 0, 0, 0, 0, 0). \tag{25}$$

The temperature in the LBM can be calculated by

$$T = \sum_{\alpha} g_{\alpha} + \frac{1}{2} q \Delta t. \tag{26}$$

In the present model, the stair-step approximation is adopted to treat a curved interface. As shown in Fig. 2, the curved interface Γ is replaced by the zigzag line Γ_0. The stair line can be divided into a series of straight line segments. As a result, the subsegments can be represented by

$$(x_{i+(1/2)}, y), y_{j-(1/2)} \leqslant y \leqslant y_{j+(1/2)}, \quad \text{or} \qquad (x, y_{j+(1/2)}), x_{i-(1/2)} \leqslant x \leqslant x_{i+(1/2)}. \tag{27}$$

At first the Dirac function is replaced by the discrete delta function. As shown in Fig. 3, two different one-dimensional discrete delta functions are used. One is [32]

$$D(x) = W_1(r) = \begin{cases} \frac{1}{3\Delta x}(1 + \sqrt{1 - 3r^2}), & 0 \leqslant |r| < 0.5, \\ \frac{1}{6\Delta x}[5 - 3|r| - \sqrt{-3(1 - |r|)^2 + 1}], & \\ 1 \leqslant |r| < 1.5, & \\ 0, |r| \geqslant 1.5. & \end{cases} \tag{28}$$

And the other is [33]

$$D(x) = W_2(r) = \begin{cases} \frac{1}{8\Delta x}(3 - 2|r| + \sqrt{1 + 4|r| - 4r^2}), & \\ 0 \leqslant |r| < 1, & \\ \frac{1}{8\Delta x}[5 - 2|r| - \sqrt{-7 + 12|r| - 4r^2}], & \\ 1 \leqslant |r| < 2, & \\ 0, |r| \geqslant 2, & \end{cases} \tag{29}$$

where $r = x/\Delta x$.

Now the calculation method of the source term q is given. Taking $q(x_i, y_j)$ as an example, we have

$$q(x_i, y_j) \approx \int_{x_{i+(1/2)}, y_{j-(1/2)}}^{x_{i+(1/2)}, y_{j+(1/2)}} \delta Q(X,Y) D(x_i - X) \delta(y_j - Y) dY + \int_{x_{i-(1/2)}, y_{j+(1/2)}}^{x_{i+(1/2)}, y_{j+(1/2)}} \delta Q(X,Y) \delta(x_i - X) D(y_j - Y) dX$$
$$+ \int_{x_{i-(1/2)}, y_{j+(1/2)}}^{x_{i-(1/2)}, y_{j-(1/2)}} \delta Q(X,Y) D(x_i - X) \delta(y_j - Y) dY + \int_{x_{i-(1/2)}, y_{j-(1/2)}}^{x_{i+(1/2)}, y_{j-(1/2)}} \delta Q(X,Y) \delta(x_i - X) D(y_j - Y) dX. \tag{30}$$

It is worth noting that in the above equation the discrete delta function W_1 is adopted. The radius of influence domain of W_1 is $1.5\Delta x$. So some other integral terms, such as $\int_{x_{i+(3/2)}, y_{j-(1/2)}}^{x_{i+(3/2)}, y_{j+(1/2)}} \delta Q(X,Y) D(x_i - X) \delta(y_j - Y) dY$, are neglected. We notice that the domains of integration in the third and fourth terms are not located at the zigzag line Γ_0. Based on the relation (7), the third and fourth terms on the right-hand side of Eq. (30) actually equal zero. Only the first and second terms must be considered. They are evaluated by

$$\int_{x_{i+(1/2)}, y_{j-(1/2)}}^{x_{i+(1/2)}, y_{j+(1/2)}} \delta Q(X,Y) D(x_i - X) \delta(y_j - Y) dY = \int_{x_{i+(1/2)}, y_{j-(1/2)}}^{x_{i+(1/2)}, y_{j+(1/2)}} \delta Q(x_{i+(1/2)}, Y) D(x_i - x_{i+(1/2)}) \delta(y_j - Y) dY$$

$$\approx D(x_i - x_{i+(1/2)}) \int_{x_{i+(1/2)}, y_{j-(1/2)}}^{x_{i+(1/2)}, y_{j+(1/2)}} \delta Q(x_{i+(1/2)}, Y)\delta(y_j - Y)dY$$
$$\approx \delta Q(x_{i+(1/2)}, y_j)D(x_i - x_{i+(1/2)})(y_{j+(1/2)} - y_{j-(1/2)}). \tag{31}$$

$$\int_{x_{i-(1/2)}, y_{j+(1/2)}}^{x_{i+(1/2)}, y_{j+(1/2)}} \delta Q(X,Y)\delta(x_i - X)D(y_j - Y)dX = \int_{x_{i-(1/2)}, y_{j+(1/2)}}^{x_{i+(1/2)}, y_{j+(1/2)}} \delta Q(X, y_{j+(1/2)})\delta(x_i - X)D(y_j - y_{j+(1/2)})dX$$
$$\approx D(y_j - y_{j+(1/2)}) \int_{x_{i-(1/2)}, y_{j+(1/2)}}^{x_{i+(1/2)}, y_{j+(1/2)}} \delta Q(X, y_{j+(1/2)})\delta(x_i - X)dX$$
$$\approx \delta Q(x_i, y_{j+(1/2)})D(y_j - y_{j+(1/2)})(x_{i+(1/2)} - x_{i-(1/2)}). \tag{32}$$

The key issue is how to calculate the heat flux δQ. In Ref. [29], a local numerical scheme for temperature derivatives is provided:

$$\nabla(\chi T) = \left\{\left(1 - \frac{\sigma_3}{2}\right)\left[\left(m_3 - m_3^{\mathrm{eq}}\right) + \frac{\sigma_4}{2}\left(m_4 - m_4^{\mathrm{eq}}\right)\right]\left(1 - \frac{\sigma_5}{2}\right)\left[\left(m_5 - m_5^{\mathrm{eq}}\right) + \frac{\sigma_6}{2}\left(m_6 - m_6^{\mathrm{eq}}\right)\right]\right\}. \tag{33}$$

Obviously, the above formula only holds when the temperature field is sufficiently smooth. However, in the present problem, when $\kappa_1 \neq \kappa_2$, we have

$$\left.\frac{\partial T_1}{\partial n}\right|_{\Gamma} \neq \left.\frac{\partial T_2}{\partial n}\right|_{\Gamma}. \tag{34}$$

So the temperature field is not smooth. Therefore the above computational scheme cannot be used in this case. Actually, the above scheme is derived using the Chapman-Enskog asymptotic analysis [30]. In the derivation of this formula, the Taylor expansion is applied for all symmetrical discrete lattice directions. It indicates that the scheme (33) is a central-difference-type scheme. Based on Appendix B in Ref. [17], we can get

$$\frac{(\chi T_x)_1 + (\chi T_x)_2}{2} = \left(1 - \frac{\sigma_3}{2}\right)\left[\left(m_3 - m_3^{\mathrm{eq}}\right) + \frac{\sigma_4}{2}\left(m_4 - m_4^{\mathrm{eq}}\right)\right], \tag{35}$$
$$\frac{(\chi T_y)_1 + (\chi T_y)_2}{2} = \left(1 - \frac{\sigma_5}{2}\right)\left[\left(m_5 - m_5^{\mathrm{eq}}\right) + \frac{\sigma_6}{2}\left(m_6 - m_6^{\mathrm{eq}}\right)\right]. \tag{36}$$

Applying Eq. (4), one can obtain

$$\kappa_1 \frac{\partial T_1}{\partial x} = \kappa_2 \frac{\partial T_2}{\partial x} = \frac{\left(1 - \frac{\sigma_3}{2}\right)\left[\left(m_3 - m_3^{\mathrm{eq}}\right) + \frac{\sigma_4}{2}\left(m_4 - m_4^{\mathrm{eq}}\right)\right]}{\frac{1}{(\rho c_p)_1} + \frac{1}{(\rho c_p)_2}}, \tag{37}$$

$$\kappa_1 \frac{\partial T_1}{\partial y} = \kappa_2 \frac{\partial T_2}{\partial y} = \frac{\left(1 - \frac{\sigma_5}{2}\right)\left[\left(m_5 - m_5^{\mathrm{eq}}\right) + \frac{\sigma_4}{2}\left(m_6 - m_6^{\mathrm{eq}}\right)\right]}{\frac{1}{(\rho c_p)_1} + \frac{1}{(\rho c_p)_2}}. \tag{38}$$

If we set

$$R_x(\mathbf{x}) = \left(1 - \frac{\sigma_3}{2}\right)\left[m_3(\mathbf{x}) - m_3^{\mathrm{eq}}(\mathbf{x})\right] + \frac{\sigma_4}{2}\left[m_4(\mathbf{x}) - m_4^{\mathrm{eq}}(\mathbf{x})\right], \tag{39}$$
$$R_y(\mathbf{x}) = \left(1 - \frac{\sigma_5}{2}\right)\left[m_5(\mathbf{x}) - m_5^{\mathrm{eq}}(\mathbf{x})\right] + \frac{\sigma_4}{2}\left[m_6(\mathbf{x}) - m_6^{\mathrm{eq}}(\mathbf{x})\right], \tag{40}$$

the heat fluxes across the interface $x_{i+(1/2)}$ and $y_{j+(1/2)}$ are given by

$$\delta Q(x_{i+(1/2)}, y_j) = \frac{2[R_x(x_i, y_j) + R_x(x_{i+1}, y_j)]\left(\frac{1}{(\rho c_p)_1} - \frac{1}{(\rho c_p)_2}\right)}{\frac{1}{(\rho c_p)_1} + \frac{1}{(\rho c_p)_2}}, \tag{41}$$

$$\delta Q(x_i, y_{j+(1/2)}) = \frac{2[R_y(x_i, y_j) + R_y(x_i, y_{j+1})]\left(\frac{1}{(\rho c_p)_1} - \frac{1}{(\rho c_p)_2}\right)}{\frac{1}{(\rho c_p)_1} + \frac{1}{(\rho c_p)_2}}. \tag{42}$$

Once $\delta Q(x_{i+(1/2)}, y_j), \delta Q(x_i, y_{j+(1/2)})$ are obtained, $q(x_i, y_j)$ can be approximated using Eqs. (30)–(32).

When considering the flow with heat transfer, the lattice Boltzmann equation (LBE) for Navier-Stokes equation is needed. The multirelaxation-time LB evolution equation for the flow field reads [34]

$$\mathbf{f}(\mathbf{x} + \mathbf{e}_\alpha \Delta t, t + \Delta t) - \mathbf{f}(\mathbf{x}, t) = -\mathbf{M}^{-1}\mathbf{S}_f[\mathbf{n}(\mathbf{x}, t) - \mathbf{n}^{\mathrm{eq}}(\mathbf{x}, t)] + \Delta t \mathbf{M}^{-1}\left(\mathbf{I} - \frac{\mathbf{S}_f}{2}\right)\mathbf{F}(\mathbf{x}, t), \tag{43}$$

where

$$\mathbf{f}(\mathbf{x},t) = (f_0(\mathbf{x},t), f_1(\mathbf{x},t), \ldots, f_8(\mathbf{x},t))^T, \quad (44)$$

$$\mathbf{n}(\mathbf{x},t) = \mathbf{M}\mathbf{f} = (n_0(\mathbf{x},t), n_1(\mathbf{x},t), \ldots, n_8(\mathbf{x},t))^T, \quad (45)$$

$$\mathbf{n}^{\mathrm{eq}}(\mathbf{x},t) = \left(n_0^{\mathrm{eq}}(\mathbf{x},t), n_1^{\mathrm{eq}}(\mathbf{x},t), \ldots, n_8^{\mathrm{eq}}(\mathbf{x},t)\right)^T, \quad (46)$$

$$\mathbf{F}(\mathbf{x},t) = (F_0(\mathbf{x},t), F_1(\mathbf{x},t), \ldots, F_8(\mathbf{x},t))^T. \quad (47)$$

The equilibrium moments $\mathbf{n}_\alpha^{\mathrm{eq}}$ are defined as

$$\mathbf{n}^{\mathrm{eq}} = (\rho, -2\rho + 3(u^2+v^2), \rho - 3(u^2+v^2), u, -u, v, -v, u^2 - v^2, uv)^T. \quad (48)$$

The diagonal relaxation matrix is expressed as

$$\mathbf{S}_f = \mathrm{diag}(s_0, s_1, s_2, s_3, s_4, s_5, s_6, s_7, s_8). \quad (49)$$

Here we set

$$s_0 = s_3 = s_5 = 0, \quad (50)$$

$$s_1 = s_2 = s_7 = s_8 = \frac{\Delta t}{3\nu/c + 0.5\Delta t}, \quad (51)$$

$$s_4 = s_6 = 8\frac{2 - s_1}{8 - s_1}. \quad (52)$$

$\mathbf{F}$ is the discrete force term in the moment space which is given as

$$\mathbf{F} = (0, 6(uf_x + vf_y), -6(uf_x + vf_y), f_x, -f_x, f_y, -f_y, 2uf_x - 2vf_y, vf_x + uf_y)^T, \quad (53)$$

where $\mathbf{f} = (f_x, f_y)$ is the body force. The macroscopic density and velocity are calculated by

$$\rho = \sum_\alpha f_\alpha, \quad (54)$$

$$\mathbf{u} = \sum_\alpha \mathbf{e}_\alpha f_\alpha + \frac{1}{2}\mathbf{f}\Delta t. \quad (55)$$

The solution procedure of the present LB scheme is provided in the following section. Suppose the physical quantities such as $g_\alpha(\mathbf{x},t)$ at time level t have been obtained. The computational procedure of the physical quantities at time level $t + \Delta t$ is summarized as follows:

(1) Compute the heat flux δQ at the interface Γ_0 using Eqs. (41)and (42).

(2) Determine the heat source q using Eqs. (30)–(32).

(3) Obtain the force term $\mathbf{F}$ and heat source or sink $\mathbf{Q}$ in LB evolution equations (43) and (16) using Eqs. (53) and (25).

(4) Compute the density and temperature distribution functions at time $t + \Delta t$ in the entire computational domain using Eqs. (43) and (16).

(5) Obtain the macroscopic velocity $\mathbf{u}$ and temperature T using Eqs. (55) and (26).

(6) Compute the equilibrium distribution functions $\mathbf{m}^{\mathrm{eq}}, \mathbf{n}^{\mathrm{eq}}$ using Eqs. (24) and (48).

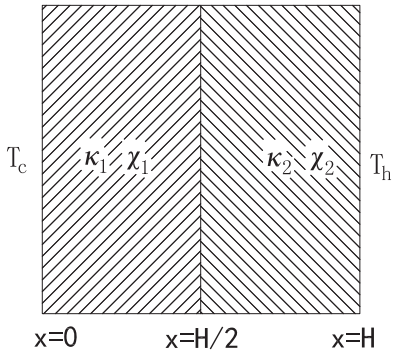

FIG. 4. Schematic of a two-layer heat conduction medium.

IV. RESULTS AND DISCUSSION

In this section, some numerical examples are simulated to verify the present LB model. To compare with the analytical solutions, three heat conduction problems which have analytical solutions are tested. Then the forced and natural convection flow problems are considered. The obtained results are also compared with the finite volume results.

A. Heat conduction in a stratified solid medium

First, the accuracy of the present interface treatment is investigated. We consider the heat conduction between two square solids which is shown in Fig. 4. The left and right walls are kept at the constant temperature $T_c, T_h (T_h > T_c)$. The periodic boundary condition is imposed on the bottom and top walls. The corresponding physical parameters are set to be $\chi_1/\chi_2 = 0.5$, $\kappa_1/\kappa_2 = 1/3$, $\sigma_{3,1} = \sigma_{5,1} = 5/3$, and $\sigma_{3,2} = \sigma_{5,2} = 10/7$. The exact solution is expressed as follows:

$$T^a(x,y) = \begin{cases} \frac{3x}{2H}(T_h - T_c) + T_c, & 0 \leqslant x \leqslant H \\ \left(\frac{x}{2H} + \frac{1}{2}\right)(T_h - T_c) + T_c, & H \leqslant x \leqslant 2H, \end{cases} \quad (56)$$

where H is the width of the computational domain. In this simulation, four different grids $\Delta x = H/20$, $H/40$, $H/80$, and $H/160$ are used. The L_2 norm is adopted to compute the dimensionless temperature numerical errors, and it is expressed as

$$L_2 \text{ error} = \frac{1}{T_h - T_c}\sqrt{\frac{\sum (T^n - T^a)^2}{N}}, \quad (57)$$

where N is the number of the node in the computational domain. As shown in Fig. 5, it can be observed that the present model has a superlinear convergence rate when different discrete delta functions are adopted. In fact, discrete delta functions lead to the first-order approximation. This conclusion has been widely validated by many IBM works. Considering the simplicity, $D = W_1$ is chosen unless stated otherwise.

Different from the work which was proposed by Wang *et al.* [19], the present method can be also applied to the unsteady conjugate heat transfer. The transient heat conduction in a three-layer stratified medium is simulated. The composite

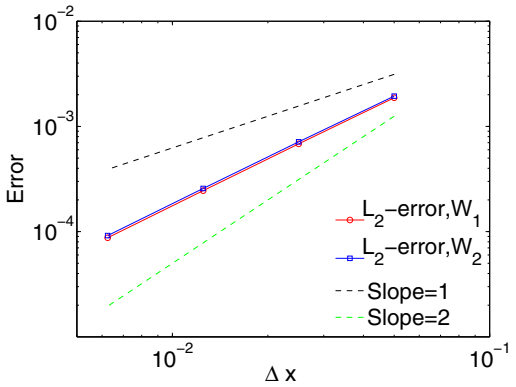

FIG. 5. (Color online) The L_2 errors of the temperature versus the grid spacing with different discrete delta functions.

medium consisting of three parallel layers is shown in Fig. 6. The initial and boundary conditions are set to be

$$T(x,y,0) = T_c, \quad 0 < x < 3H, \quad 0 < y < 1.5H, \tag{58}$$

$$T(x,0,t) = T(x,1.5H,t), \tag{59}$$

$$T(0,y,t) = T_c, \quad T(3H,y,t) = T_h. \tag{60}$$

In Ref. [35], a series solution is provided. The numerical solution will be compared with the analytical solution. In this simulation, the corresponding parameters are set as $\chi_1 = \chi_3 = 1.0$, $\chi_2 = 3.0$, $\kappa_1 = \kappa_3 = 1.0$, $\kappa_2 = 0.1$, $\sigma_{3,1} = \sigma_{5,1} = 5/3$, $\sigma_{3,2} = \sigma_{5,2} = 1.25$, and $\sigma_{3,3} = \sigma_{5,3} = 5/3$. A mesh which consists of 90×90 cells is used. In Fig. 7, the dimensionless temperature profiles $(T - T_h)/\Delta T$ at the times $t = 0.1,0.5,1,2$ are plotted, where $\Delta T = T_h - T_c$. As can been seen, the numerical results have excellent agreement with the analytical solutions. This phenomenon indicates that the present method is capable of simulating the unsteady conjugate heat transfer.

B. Heat conduction in concentric annulus

Now we consider the heat conduction problem with curved boundaries. The concentric annulus with different thermodynamic parameters is shown in Fig. 8. The following Dirichlet boundary condition is imposed on the outer cylinder:

$$T(R_2,\theta) = \cos[n(\theta + \theta_0)], \quad n \in \mathbb{Z}, \tag{61}$$

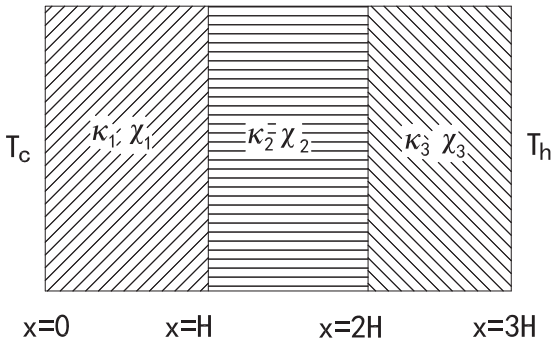

FIG. 6. Schematic of a three-layer stratified medium.

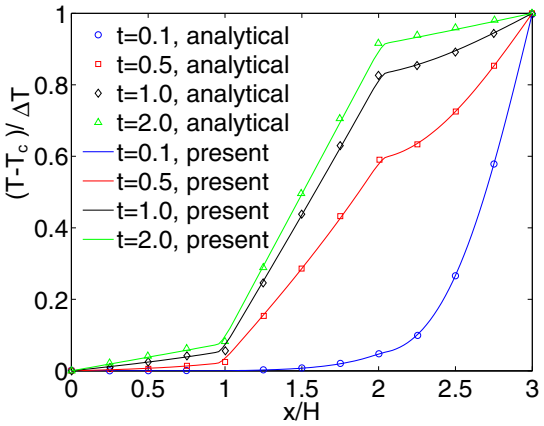

FIG. 7. (Color online) Comparison of the analytical and LBM solutions at different times.

where R_2 is the radius of the outer cylinder and the inner boundary is subjected to the following conjugate boundary condition:

$$T_1(R_1) = T_2(R_1), \tag{62}$$

$$\kappa_1 \frac{\partial T_1}{\partial r}(R_1) = \kappa_2 \frac{\partial T_2}{\partial r}(R_1), \tag{63}$$

where R_1 is the radius of the inner cylinder.

The analytical solution for this problem is given by [23]

$$T_1^e(r,\theta) = c_1 r^n \cos[n(\theta + \theta_0)], \quad 0 \leqslant r \leqslant R_1, \tag{64}$$

$$T_2^e(r,\theta) = (c_2 r^n + c_3 r^{-n}) \cos[n(\theta + \theta_0)], \quad R_1 \leqslant r \leqslant R_2, \tag{65}$$

where

$$c_1 = \frac{2\kappa_2/\kappa_1 R_1^{-2n} R_2^{-n}}{(\kappa_2/\kappa_1 + 1)R_1^{-2n} + (\kappa_2/\kappa_1 - 1)R_2^{-2n}}, \tag{66}$$

$$c_2 = \frac{(\kappa_2/\kappa_1 + 1)R_1^{-2n} R_2^{-n}}{(\kappa_2/\kappa_1 + 1)R_1^{-2n} + (\kappa_2/\kappa_1 - 1)R_2^{-2n}}, \tag{67}$$

$$c_3 = \frac{(\kappa_2/\kappa_1 - 1)R_2^{-n}}{(\kappa_2/\kappa_1 + 1)R_1^{-2n} + (\kappa_2/\kappa_1 - 1)R_2^{-2n}}. \tag{68}$$

In the present method, the smooth curved surface is assumed to be zigzag lines; the accuracy of the boundary

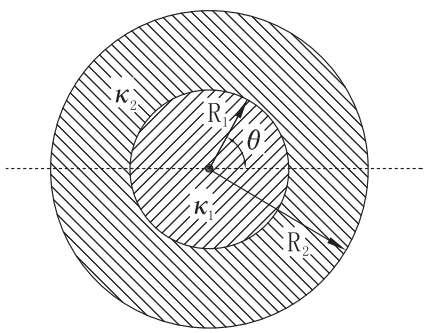

FIG. 8. Schematic illustration of a two-layer annulus.

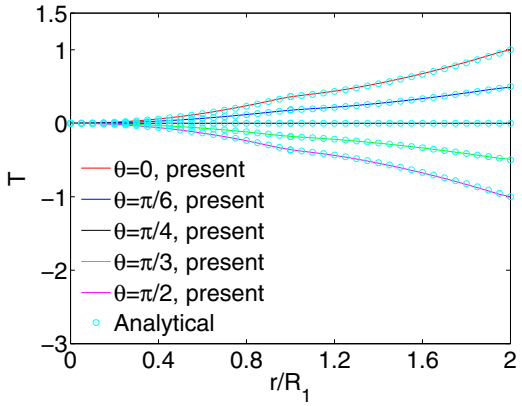

(a) $\kappa_2/\kappa_1 = 3$

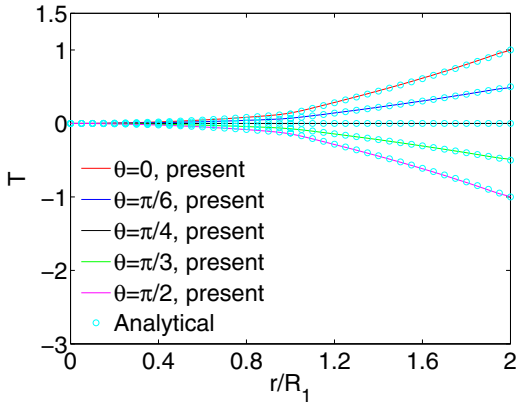

(b) $\kappa_2/\kappa_1 = 1/3$

FIG. 9. (Color online) Comparison of the present radial temperature profiles with analytical solutions when $\theta = 0,\pi/6,\pi/4,\pi/3,\pi/2$ and $\theta_0 = 0$.

approximation is consistent with that of the discrete delta approximation. The corresponding parameters for this simulation are set to be $n = 2$, $R_2 = 2R_1$, $\chi_1 = \chi_2 = 0.8$, $\kappa_2/\kappa_1 = 3$ or $1/3$, $\sigma_{3,1} = \sigma_{5,1} = 1.25$, and $\sigma_{3,2} = \sigma_{5,2} = 1.25$. The numerical results are obtained from simulations on a 100×100 mesh. In addition, the Dirichlet boundary condition on the outer cylinder must be treated. Here the immersed boundary method which was proposed in Ref. [17] is used.

Figure 9 presents the radial temperature profiles for different thermal conductivity ratios at $\theta = 0,\pi/6,\pi/4,\pi/3,\pi/2$ when $\theta_0 = 0$. As expected, the LBM results show good agreement with the analytical solutions. Considering the stair-step approximation of the curved interface, the representation of the interface geometry is not accurate. So the rotational symmetry of the present method is tested. The outer cylinder is imposed on three different boundary conditions (61) with $\theta_0 = 0, -\pi/6, -\pi/4$. The radial temperature profiles at $\theta = 0,\pi/6,\pi/4$ ($\theta + \theta_0 = 0$) are presented in Fig. 10. It can be seen clearly that these results are very close to each other. This indicates that the present method is adequate to deal with the heat transfer problem in complex geometries.

C. Forced convection in a channel

In this section, the flow and heat transfer in a channel is simulated as an example to illustrate the practical application of the

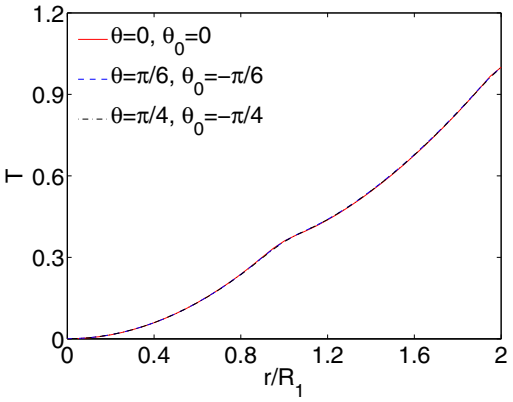

FIG. 10. (Color online) Comparison of the radial temperature profiles when $\kappa_2/\kappa_1 = 3$. Red solid line: $\theta = 0$, $\theta_0 = 0$. Blue dashed line: $\theta = \pi/6$, $\theta_0 = -\pi/6$. Black dash-dotted line: $\theta = \pi/4$, $\theta_0 = -\pi/4$.

present method. As shown in Fig. 11, the sizes of both fluid and solid domains are $4H \times H$, where H is the width of the channel. The outer boundaries of the solid domain are heated by high temperature T_h. The left and right boundaries of the solid domain are adiabatic. At the inlet, the fluid with a low temperature T_c is injected. The flow is driven by the pressure flow and is assumed to be a fully developed state. In other words, the flow in the channel has the following analytical solution:

$$u(x,y) = 4u_0\left(\frac{y}{H} - 1\right)\left(2 - \frac{y}{H}\right), \quad H \leqslant y \leqslant 2H, \tag{69}$$

where u_0 is the peak velocity in the channel.

The cases with two different thermal conductivity ratios between solid and fluid phases ($\kappa_s/\kappa_f = 3,10$) are simulated. When $\kappa_s/\kappa_f = 3$, we have $\sigma_{3,s} = \sigma_{5,s} = 1.25$ and $\sigma_{3,f} = \sigma_{5,f} = 5/3$. On the other hand, as $\kappa_s/\kappa_f = 10$, the corresponding parameters are set to be $\sigma_{3,s} = \sigma_{5,s} = 2/3$ and $\sigma_{3,f} = \sigma_{5,f} = 5/3$. To compare different numerical results, the conventional finite volume method (SIMPLE -like algorithm) is also used to simulate the present problem. Both simulations are carried out on a 160×120 mesh. In finite volume (FV) simulation, the peak velocity is fixed at $u_0 = 1$. Actually, different from LBM, no low Mach number limit exists in the conventional FV scheme. As shown in Fig. 12, the

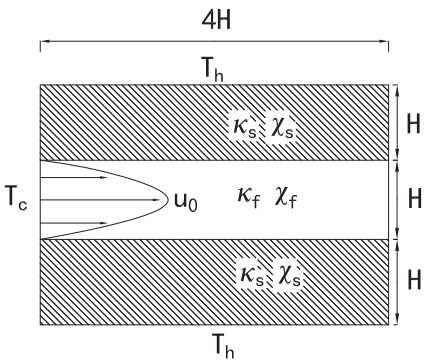

FIG. 11. Schematic illustration of flow and heat transfer in a channel.

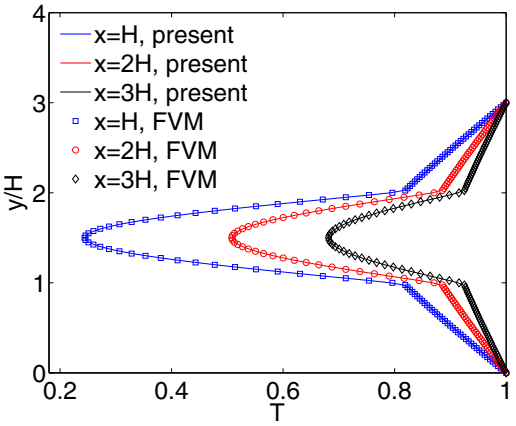

(a) $\kappa_s/\kappa_f = 10$

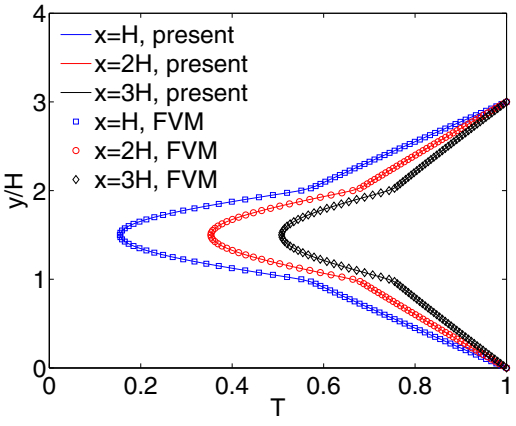

(b) $\kappa_s/\kappa_f = 3$

FIG. 12. (Color online) Comparison of the temperature profiles for different thermal conductivity ratios at different horizontal positions: $x/H = 1,2,3$.

temperature profiles at different horizontal positions $x/H = 1,2,3$ are presented. An overview of the figure indicates that the LBM results show excellent agreement with the FV results. Furthermore, we find that the relative errors of the temperature (max $\frac{T_{\mathrm{LBM}}-T_{\mathrm{FV}}}{T_{\mathrm{FV}}}$) between different methods are within 0.56%. Because the finite volume method (FVM) (SIMPLE -like algorithm) has been well verified in the previous work, it indicates that the present LB scheme is suitable for simulating conjugate heat transfer problems. The CPU time costs for both methods are also compared on the same mesh. The present simulations are running on a desktop (CPU 3.4 GHz and 8 G RAM). Only serial programs are considered. For the present problem, the FV scheme is almost 2.31 times faster than the present LBE. This is consistent with the conclusion in Ref. [36]. However, the LBM is intrinsically parallel. The parallel LBM codes are more efficient. For the practical applications, heat transfer in complex geometries can be encountered frequently. In this case, the LBM has a great advantage over the FVM [36].

D. Natural convection in a cavity filled with circular solid blocks

The present method is also extended to simulate the natural convection with conjugate heat transfer. Different from the forced convection, the velocity and temperature fields are coupled in the natural convective flow. Figure 13 depicts a schematic of a cavity filled with circular solid blocks. The bottom and top walls are adiabatic. The left wall is heated uniformly and right is cooled uniformly ($T_h > T_c$). The cavity is filled with some conducting solid blocks in the form of circular obstacles of diameter d_p. The void space is filled with the fluid. Under the gravity condition, the convective flow is driven by the temperature difference. For the natural convection, two important parameters, Rayleigh and Prandtl numbers, must be defined. They are

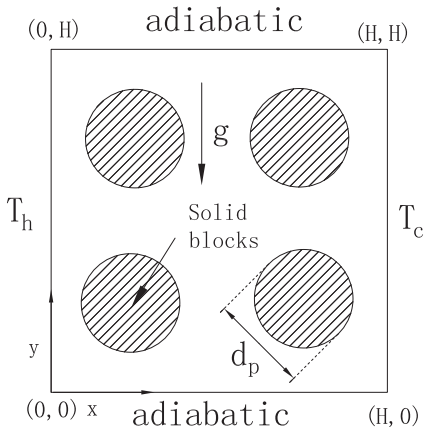

FIG. 13. Schematic of a cavity filled with solid blocks.

$$\mathrm{Ra} = \frac{g\beta H^3(T_h - T_c)}{\nu\chi_f}, \quad \mathrm{Pr} = \frac{\nu}{\chi_f}, \tag{70}$$

where g,β are the gravitational acceleration and thermal expansion coefficients of the fluid, respectively, H is the side length of the cavity, and ν is the kinematic viscosity of the fluid.

Moreover, the porosity ϕ is calculated as

$$\phi = 1 - N\frac{\pi d_p^2}{4H^2}, \tag{71}$$

where N is the number of blocks. The Nusselt number which evaluates the heat transfer rate is given by

$$\mathrm{Nu} = -\frac{H}{(T_h - T_c)}\frac{\partial T}{\partial x}\bigg|_{x=0}. \tag{72}$$

The average Nusselt number is computed by

$$\bar{\mathrm{Nu}} = \frac{\int_0^H Nu\, dy}{H}. \tag{73}$$

The no-slip boundary condition on the surfaces of the inner cylinders is implemented using the immersed boundary

TABLE I. Comparison of the averaged Nusselt number when $\mathrm{Ra} = 10^5$, $\mathrm{Pr} = 0.7$, $\chi_s/\chi_f = 1$.

κ_s/κ_f	LBM	FVM
0.1	0.8495	0.8503
1	1.2614	1.2986
10	2.0429	2.0375
100	2.2957	2.2656

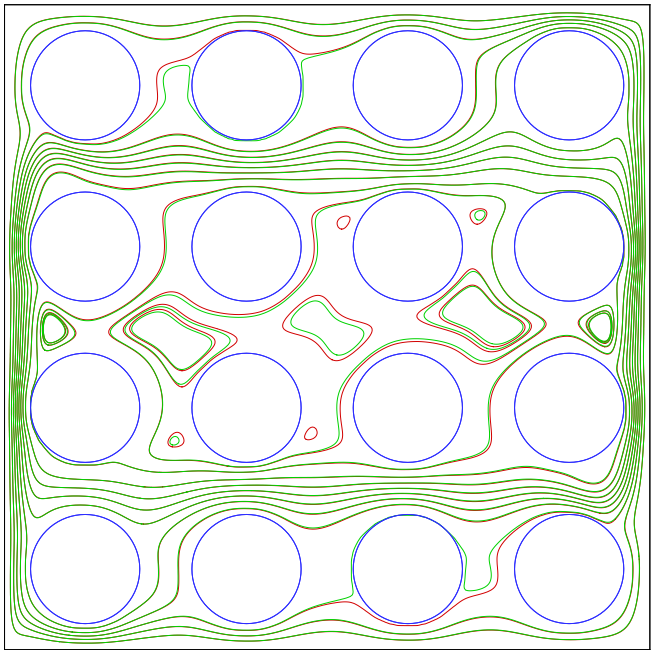

(a) $\kappa_2/\kappa_1 = 3$

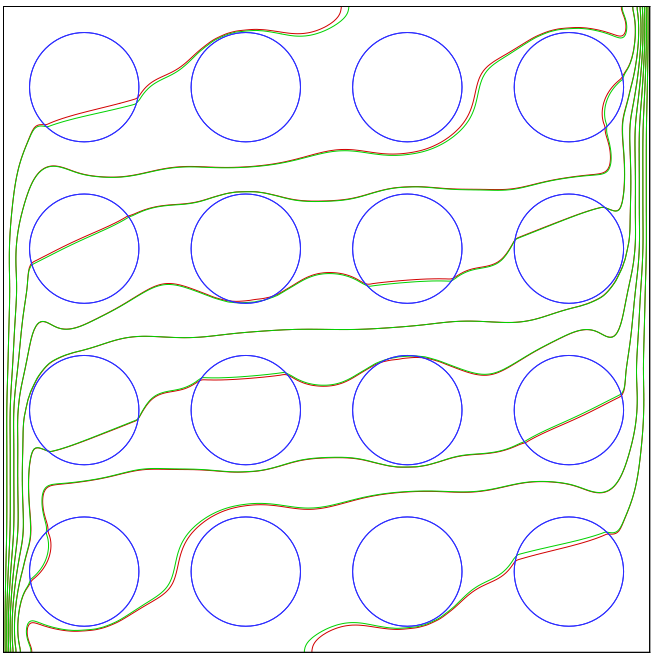

(b) $\kappa_2/\kappa_1 = 1/3$

FIG. 14. (Color online) Comparison of LBM results (red lines) and FVM results (greenish-gray lines): (a) streamlines and (b) isotherms, for Ra $= 10^5$, Pr $= 0.7$, $\phi = 0.64$, $\kappa_s/\kappa_f = 5$, $N = 4$.

method in Ref. [37]. Now we consider the cases with Ra $= 10^5$, Pr $= 0.7$, $\chi_s/\chi_f = 1$, $N = 4$, and $\phi = 0.64$ for different thermal conductivity ratios. The simulation parameters are set to be $\sigma_{3,s} = \sigma_{5,s} = 1.25$ and $\sigma_{3,f} = \sigma_{5,f} = 1.25$. We also employ the FVM (SIMPLE-like algorithm) and pseudo-solid-specific-heat technique to simulate the present thermal flow problem on 200×200 mesh. Both LBM results and FV results of the averaged Nusselt number are listed in Table I. It can be seen obviously that $\bar{\text{Nu}}$ increases with the increasing of κ_s/κ_f. Good agreement between the two calculation results can be observed.

Finally, the present LB model is used to investigate the effect of the number N. ϕ and Pr are also set to be 0.64,0.7. The number of cylinders N is increased from 4×4 to 32×32. Ra is fixed at 10^7. The thermal conductivity ratio κ_s/κ_f is set to be 5. Accordingly, $\sigma_{3,s} = \sigma_{5,s} = 10/11$ and $\sigma_{3,f} = \sigma_{5,f} = 5/3$ are chosen.

To compare the LB results and FV results more fully, the streamlines and isotherm for $N = 4 \times 4$ are presented in Fig. 14. Some small eddies are be captured by two methods. It can be found that there are no significant differences between the two results. Figure 15 depicts the streamlines and isotherms for $N = 8 \times 8, 16 \times 16, 32 \times 32$. When $N = 8 \times 8$, the isotherms are irregular. As N increases, the isotherms become smoother. In fact, as the number of cylinders increases, the flow and temperature field can be studied using a semiempirical method at the representative elementary volume scale [12–14].

V. CONCLUSIONS

Study of the conjugate heat transfer using LBM has been a hot topic over the last two years [23,25–27]. In fact, two different strategies have been considered to deal with this issue. The first strategy is to discretize Eqs. (3) and (4) directly [23,25,26]. Then the distribution functions neighboring the interface can be corrected. However, these algorithms depend on the the topology of the interface. Complicated treatments are needed to satisfy the conjugate boundary conditions. The other strategy is to introduce a source term in the evolution equation [27]. The source term method is very simple and efficient. However, in the work of Karani and Huber [27], their method is a lack of mathematical rigor in differentiating a piecewise constant function. Moreover, the dependency between the finite difference scheme of heat capacitance and numerical solutions exists. In this work, we propose a new source term method to implement the conjugate interface conditions based on LBE. A unified governing equation with a source term is built in different regions. Through a simple mathematical demonstration, we prove that the conjugate interface conditions can be satisfied. The present LB model is based on a rigorous mathematical foundation. Furthermore, the curved interface is assumed as zigzag lines. So the off-lattice points do not exist in this model. The present model can be viewed as a full Eulerian method. As a result, many complex thermal flow problems with conjugate heat transfer, such as the phase change problems and the coupled multiple physicochemical thermal processes, can be simulated efficiently. The conjugate interface conditions hold instantaneously. So the present model can be employed for both steady and transient conjugate heat transfer problems.

This LB model has been validated through several test examples, including both steady and unsteady conjugate heat transfer. It can be found that the obtained results show good agreement with the analytical or finite volume solutions. In particular, two practical applications have been considered: cooling of the microchannel and natural convection in a

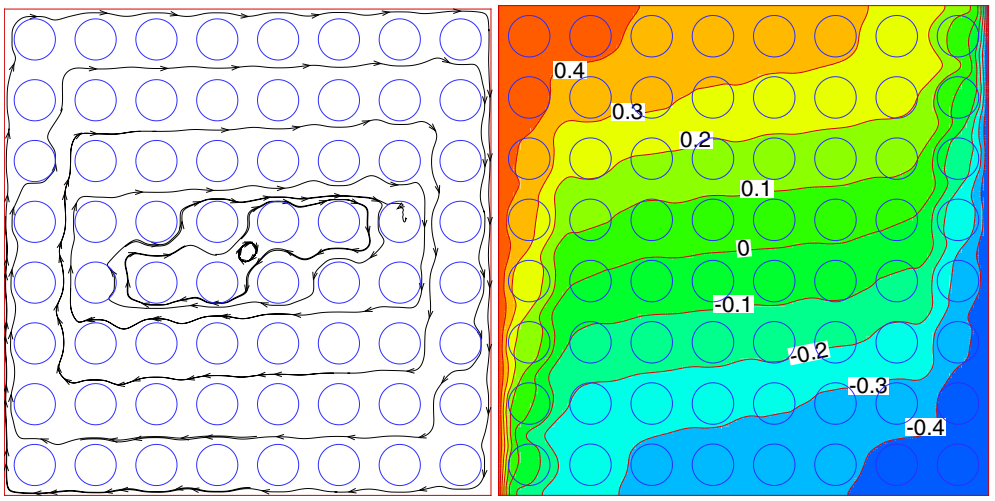

(a) $N = 8$

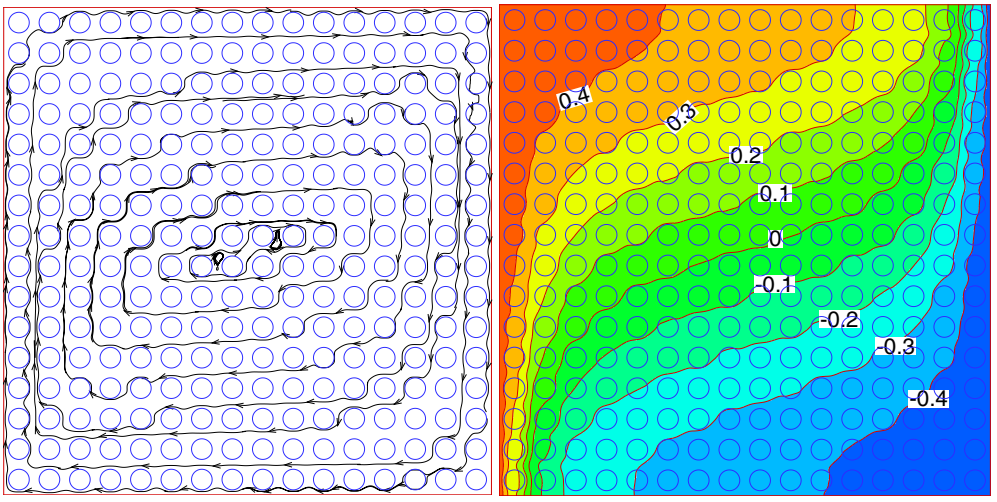

(b) $N = 16$

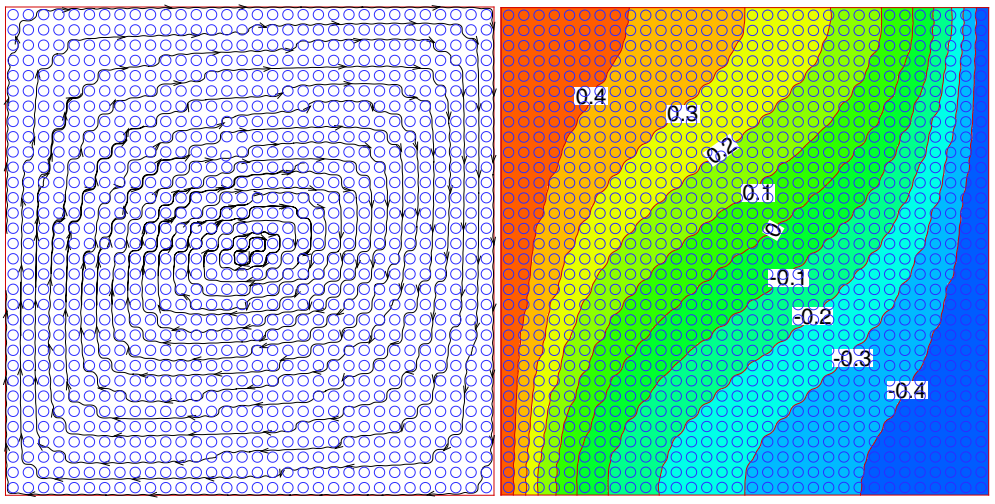

(c) $N = 32$

FIG. 15. (Color online) Streamlines and isotherms for Ra $= 10^5$, Pr $= 0.7$, $\phi = 0.64$, $\kappa_s/\kappa_f = 5$.

porous enclosure. These numerical tests clearly indicate that the present conjugate interface treatment has a strong application potential.

It should noted that only two-dimensional cases are mentioned in this paper. The three-dimensional lattice Botzmann models can be constructed similarly.

ACKNOWLEDGMENTS

This research was supported by the National Natural Science Foundation of China (Grant No. 51375039), Beijing Natural Science Foundation (Grant No. 4142046), and Program for Changjiang Scholars and Innovative Research Team (Grant No. IRT13046).

[1] X. Shan and H. Chen, Phys. Rev. E **47**, 1815 (1993).
[2] X. Y. He, S. Y. Chen, and R. Zhang, J. Comput. Phys. **152**, 642 (1999).
[3] C. M. Teixeira, Int. J. Mod. Phys. C **9**, 1159 (1998).
[4] H. Yu, S. S. Girimaji, and L. S. Luo, J. Comput. Phys. **209**, 599 (2005).
[5] X. Nie, G. D. Doolen, and S. Chen, J. Stat. Phys. **107**, 279 (2002).
[6] C. Y. Lim, C. Shu, X. D. Niu, and Y. T. Chew, Phys. Fluids **14**, 2299 (2002).
[7] Z. Feng and E. Michaelides, J. Comput. Phys. **195**, 602 (2004).
[8] H. Z. Yuan, X. D. Niu, S. Shu, M. J. Li, and H. Yamaguchi, Comput. Math. Appl. **67**, 1039 (2014).
[9] H. Z. Yuan, S. Shu, X. D. Niu, M. J. Li, and Y. Hu, Adv. Appl. Math. Mech. **6**, 307 (2014).
[10] H. Zhang, Y. Q. Tan, S. Shu, X. D. Niu, F. X. Trias, D. M. Yang, H. Li, and Y. Sheng, Comput. Fluids **94**, 37 (2014).
[11] Y. Hu, D. C. Li, S. Shu, and X. D. Niu, Phys. Rev. E **91**, 033301 (2015).
[12] Z. Guo and T. S. Zhao, Phys. Rev. E **66**, 036304 (2002).
[13] L. Chen, W. Fang, Q. Kang, J. De'Haven Hyman, H. S. Viswanathan, and W.-Q. Tao, Phys. Rev. E **91**, 033004 (2015).
[14] Y. Hu, D. C. Li, S. Shu, and X. D. Niu, Int. J. Heat Mass Transfer **92**, 1166 (2016).
[15] X. He, S. Chen, and G. D. Doolen, J. Comput. Phys. **146**, 282 (1998).
[16] Y. Hu, X. D. Niu, S. Shu, H. Z. Yuan, and M. J. Li, Adv. Appl. Math. Mech. **5**, 321 (2013).
[17] Y. Hu, D. C. Li, S. Shu, and X. D. Niu, Int. J. Heat Mass Transfer **81**, 591 (2015).
[18] Y. Hu, D. C. Li, S. Shu, and X. D. Niu, Int. Commun. Heat Mass Transfer, **68**, 188 (2015).
[19] J. Wang, M. Wang, and Z. Li, Int. J. Therm. Sci. **46**, 228 (2007).
[20] A. Tarokn, A. A. Mohamad, and L. Jiang, Numer. Heat Transfer, Part A **63**, 159 (2013).
[21] F. Meng, M. Wang, and Z. Li, Int. J. Heat Fluid Flow **29**, 1203 (2008).
[22] M. Seddiq, M. Maerefat, and M. Mirzaei, Int. J. Therm. Sci. **75**, 28 (2014).
[23] L. Li, C. Chen, R. Mei, and J. F. Klausner, Phys. Rev. E **89**, 043308 (2014).
[24] Y. Hu, D. C. Li, S. Shu, and X. D. Niu, Comput. Math. Appl. **70**, 2227 (2015).
[25] K. Guo, L. Li, G. Xiao, N. AuYeung, and R. Mei, Int. J. Heat Mass Transfer **88**, 306 (2015).
[26] G. Le, O. Oulaid, and J. Zhang, Phys. Rev. E **91**, 033306 (2015).
[27] H. Karani and C. Huber, Phys. Rev. E **91**, 023304 (2015).
[28] H. Yoshida and M. Nagaoka, J. Comput. Phys. **229**, 7774 (2010).
[29] Z. Chai and T. S. Zhao, Phys. Rev. E **87**, 063309 (2013).
[30] R. Huang and H. Wu, J. Comput. Phys. **274**, 50 (2014).
[31] R. Huang and H. Wu, J. Comput. Phys. **277**, 305 (2014).
[32] A. M. Roma, C. S. Peskin, and M. J. Berger, J. Comput. Phys. **153**, 509 (1999).
[33] C. S. Peskin, Acta Numer. **11**, 479 (2002).
[34] P. Lallemand and L. S. Luo, Phys. Rev. E **61**, 6546 (2000).
[35] Y. Sun and I. S. Wichman, Int. J. Heat Mass Transfer **47**, 1555 (2004).
[36] J. Bernsdorf, F. Durst, and M. Schäfer, Int. J. Numer. Meth. Fluids **29**, 251 (1999).
[37] Y. Hu, H. Z. Yuan, S. Shu, X. D. Niu, and M. J. Li, Comput. Math. Appl. **68**, 140 (2014).